

# AFM Study of the Dielectric Breakdown in Ta<sub>2</sub>O<sub>5</sub> Films

L. Vázquez, I. Montero,\* and J. M. Albella

*Instituto Ciencia de Materiales, CSIC & Dept. Física Aplicada,  
UAM Cantoblanco, 28049 Madrid, Spain*

*Received March 31, 1995. Revised Manuscript Received June 26, 1995\**

High-resolution images, at nanometric scale, of the damage produced on anodic Ta<sub>2</sub>O<sub>5</sub> oxide films subjected to breakdown during anodic oxidation have been obtained by atomic force microscopy (AFM). The time evolution of the breakdown damage has been followed by anodizing different samples at increasing anodization times after breakdown. The AFM images reveal that the breakdown is initiated at definite spots scattered all across the surface of the oxide, producing a granular structure of about 100 nm diameter. Superimposed on this granular structure some protrusions of larger sizes also appear which, after further anodization, give rise to ridges and craters on the surface. The damaged areas are then propagated in the form of branches covering large regions of the oxide surface. The evolution of the tantalum oxide during the double-anodization experiments was also studied. Healing effects of the breakdown damage has been directly observed and related to the decrease of the electron avalanches causing the breakdown. The AFM images have been also used to quantify the variation of the surface roughness of samples anodized in different conditions.

## Introduction

Anodic oxide films of tantalum are widely used as dielectric layers in electronic devices such as electrolytic and thin film capacitors. Other applications in metal oxide semiconductor (MOS) structures for microelectronic circuits are under study. Numerous attempts have been made to obtain thicker films during the growing process of the oxide in order to increase the voltage range that can be sustained by the dielectric layer under stable conditions. In this regard, the electrolytic breakdown in anodic oxide films has traditionally appeared as a phenomenon of great interest since it imposes a limit to the maximum thickness attainable for the oxide growth. The phenomenon is complex and at present there are not definite models to explain all the local events succeeding at the breakdown spots (avalanches, localized Joule heating, melting and evaporation, recrystallization, etc.). Anodically formed films of Ta<sub>2</sub>O<sub>5</sub> are amorphous when formed at voltages below breakdown, but upon heating at temperatures above 700 °C, they can recrystallize to other disordered forms.<sup>1,2</sup> Likewise, the breakdown processes occurring during the anodization at high voltages also produce structural changes in the oxide film, namely, from the amorphous state to other crystalline structures.

Generally, the breakdown damage produced on the surface of the samples has been observed by optical microscopy and scanning electron microscopy (SEM). However, low-resolution images can be obtained by SEM due to charging effects on the insulator films. On the other hand, atomic force microscope (AFM) provides a useful tool that allows not only direct surface observation, with tridimensional imaging at nanometric resolu-

tion, but also quantification of the surface roughness. The present work has been undertaken to investigate the first stages and the evolution of the breakdown phenomenon during the anodic oxidation using this novel technique. To our knowledge, this is the first time this technique is reported on the observation of the breakdown damage.

## Experimental Procedure

Tantalum foils of 99.96% nominal purity were anodized galvanostatically at room temperature up to the breakdown voltage in a standard electrolytic cell. The current density was 2.0 mA cm<sup>-2</sup>, and the electrolyte was phosphoric acid (H<sub>3</sub>PO<sub>4</sub>) solved in deionized water at two extreme concentrations: 0.001 M (*E<sub>an</sub>*) and 1.0 M (*E<sub>con</sub>*). Previous to anodization, the surface of the samples was first degreased and chemically polished in a mixture of concentrated H<sub>2</sub>SO<sub>4</sub>, HNO<sub>3</sub>, and HF in a 5:2:2 volume ratio and then in a buffered solution of NH<sub>4</sub>F in HF. The specimens were finally washed in deionized water. After this treatment, the surface of the foil exhibited small crystals separated by grain boundaries, forming a mosaic-like structure. In all cases, the anodization and breakdown voltages reported in this paper correspond to the voltage applied across the oxide film, i.e., once the electrolyte drop in the cell has been corrected.

The oxide surface was observed by AFM using a Nanoscope III system (Digital Instruments) operating in the contact mode. Silicon nitride cantilevers were employed. All images were acquired at a resolution of 512 × 512 pixels. To obtain representative images of the surface, we scanned wide areas (typically 60 μm, although sometimes we scanned 110 μm) and then we reduced the scan size. Thus, images of 60, 25, 10, and 3 μm were taken for every sample. From each image the root-mean-square (rms) roughness was calculated. The AFM images presented in this paper are offered either as a top view (the brighter the pixel the larger the height) or as a three-dimensional representation.<sup>3</sup> The interpretation of AFM images is often complicated by distortions resulting from the nonnegligible size of the probe tip. In particular, angular surface features tend to be distorted by convolution with the surface of the tip. This can be important when imaging the deepest pores, having diameters similar to the probe. Under

\* Abstract published in *Advance ACS Abstracts*, August 1, 1995.

(1) Pawel, R. E.; Campbell, J. J. *J. Electrochem. Soc.* **1984**, *111*, 1230.

(2) Stephenson, N. C.; Roth, R. S. *J. Solid State Chem.* **1971**, *3*, 145.

(3) Quate, C. F. *Surf. Sci.* **1994**, *299/300*, 980.

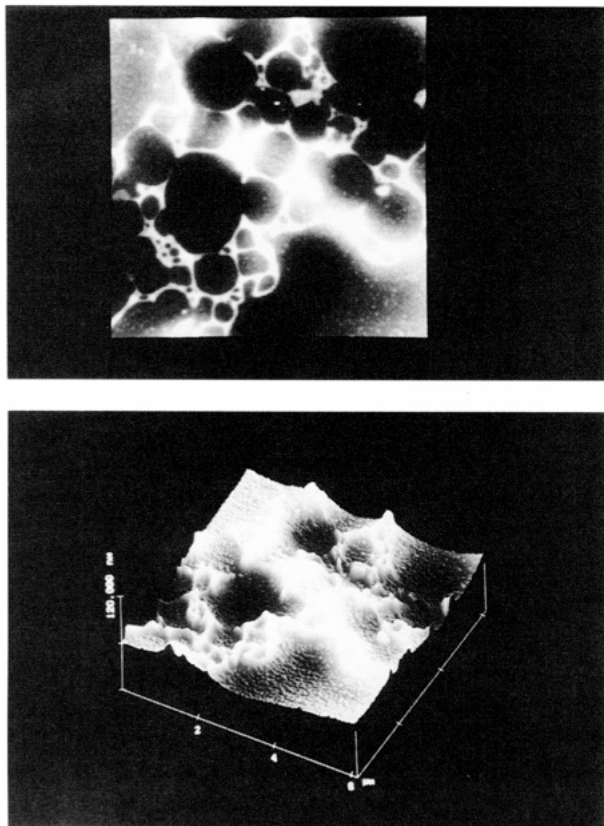


**Figure 1.** The  $6 \times 6 \mu\text{m}^2$  AFM images of the oxide surface at the initial stages of breakdown: (a, top) top view, (b, bottom) tridimensional (3D) representation. Note that the  $z$  scale has been magnified in order to enhance the surface morphology.

these circumstances, the topography of the images tends to underestimate the sharpness and depth of the pores, showing in these cases a wall slope of about  $55^\circ$ , i.e., the silicon nitride tip angle. Although some other artifacts are occasionally observed, they are in most cases significantly smaller than the features described below.

### Results

As it is known during the anodic oxidation process of tantalum at a constant current density, the thickness of the oxide grows almost linearly with time until the dielectric breakdown occurs. The oxidation process at high voltages, below breakdown, produces in all cases a smoothing of the mosaic structure of the surface. When the voltage attains the breakdown voltage,  $V_B$ , a sustained sparking appears, and the evolution of the oxide surface is the following:

(i) During the initial stages of the breakdown the surface shows rough spots or protrusions (about 6–10 nm high), encircling small valleys, which are interconnected in branches, covering wide areas of the surface. Figure 1 shows an example of this behavior. In this case the sample was anodized in the dilute electrolyte at a voltage  $V = 330$  V, which is somewhat higher than the breakdown voltage in this electrolyte ( $V_B = 320$  V). Surprisingly, no pores or microfissures are observed at this stage, although small grains appear scattered on the flat areas of the surface, with a typical size of 70–150 nm diameter and 2–4 nm height (Figure 1b). It is worth noting that such small corrugations are hardly distinguishable in SEM images.

(ii) Further anodization of the sample at  $V = 380$  V gives rise to a well-defined structure of cracks and

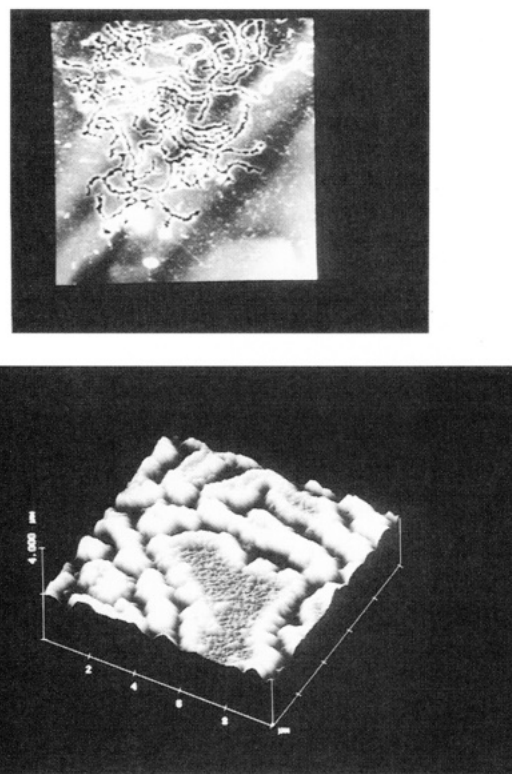


**Figure 2.** (a, top)  $60 \times 60 \mu\text{m}^2$  AFM image and (b, bottom) 3D representation at higher resolution ( $10 \times 10 \mu\text{m}^2$ ) of the breakdown damage of a sample anodized at 380 V.

microfissures running in branches across the oxide surface, as observed in Figure 2. The measured depth of the fissures is about  $0.4 \mu\text{m}$  with a width of  $1.1 \mu\text{m}$ , the total thickness of the oxide being  $0.6 \mu\text{m}$ . Some probe artifacts, as mentioned above, may underestimate these values. In any case, these results indicate the formation of nonshorting pores. In the flat areas is observed the same fine granular structure as in the previous images, but the grains are larger in diameter and distributed in different sizes, namely, 200–300 nm wide and 20–150 nm high.

(iii) Prolonged anodization at higher voltages produces the so-called “gray oxide”. The sample shows in this case wider cracks and grains extended all across the surface. The greater size of the cracks is likely associated to the coalescence of the multiple microfissures present in the surface (Figure 3).

An assessment of the breakdown damage produced at different anodization times has been made through roughness measurements of the oxide surface on representative breakdown areas. Figure 4 shows the roughness of the sample as a function of the anodization time. The roughness values were directly obtained from the software supplied by the AFM instrument. As can be appreciated, before breakdown the roughness of the oxide surface slightly decreases with the formation voltage (or, equivalently, the oxide thickness) as a consequence of the smoothing effect of the oxide growth. However, for voltages above breakdown the roughness suddenly increases with time (up to 60%), due to the surface damage.

It is worth mentioning that samples not chemically etched, i.e., showing the typical rolling grooves characteristic of the lamination process of the foil, present a lower breakdown voltage and a distinct breakdown

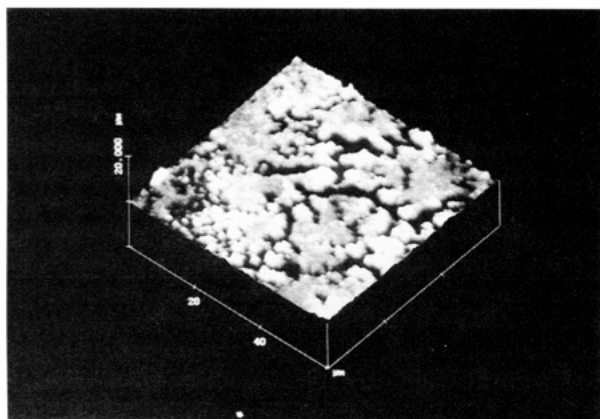


**Figure 3.** A  $60 \times 60 \mu\text{m}^2$  3D representation of an AFM image of a sample subjected to prolonged anodization after breakdown, showing the characteristic "gray oxide".

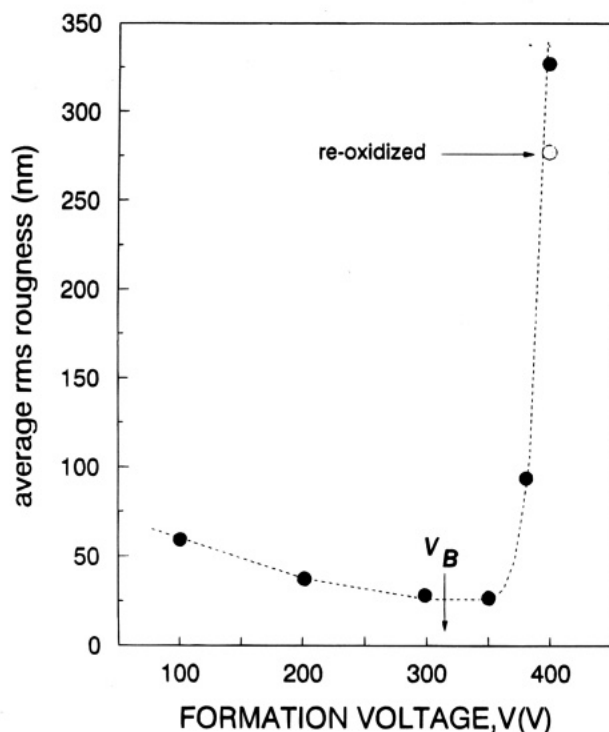


**Figure 4.** Root-mean-square (rms) surface roughness of  $25 \times 25 \mu\text{m}^2$  images of samples subjected at different stages of anodization and breakdown.

morphology. Figure 5 shows a top view of a sample after the breakdown process at two different voltages,  $V = 330$  and  $380$  V (Figure 5a,b, respectively). In Figure 5a is observed the formation of isolated pores distributed in different sizes (diameter in the 280–450 nm range). These pores are preferentially aligned along the rolling lines. For long breakdown times the pores are deeper and larger, covering almost all the surface of the sample (Figure 5b). However, in this case, the granular structure is not so apparent as in the chemically etched samples. Additionally, no crack fingers or microfissures were observed.

To study the healing effects associated to the breakdown discharges, we performed "double anodization" experiments, i.e., samples subjected to dielectric breakdown were reanodized under different conditions of the previous anodization. As is known, the sequential formation of the oxide film in different electrolytes produces a breakdown voltage that is a function only of

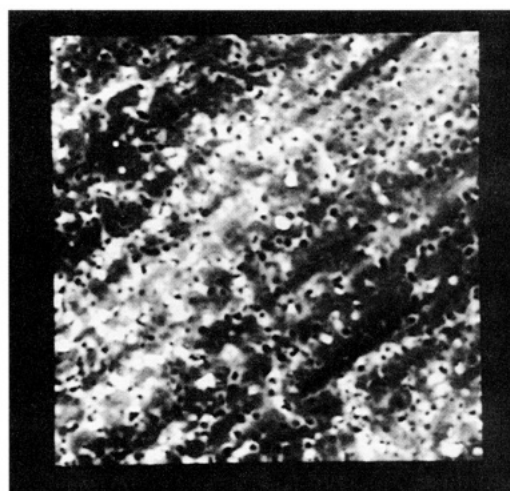


**Figure 5.** The  $25 \times 25 \mu\text{m}^2$  AFM images of a sample not chemically etched subjected to breakdown at  $V = 330$  V (a, top) and  $V = 380$  V (b, bottom).

the last electrolyte. Furthermore, in the reanodization experiments, if the oxide is first formed up to the breakdown voltage, the change of the electrolyte results in a new voltage–time curve characteristic of the last electrolyte. This implies that the oxide breakdown properties are mainly controlled at the electrolyte/oxide interface.<sup>4</sup>

In a first set of experiments, samples previously broken down at  $380$  V in the dilute electrolyte were reanodized under the same conditions up to a constant voltage,  $V = 300$  V, lower than the breakdown voltage. The samples were then left at this constant voltage (potentiostatic conditions) for a fixed time (3 h, Figure 6a). In another series of experiments, the oxidation in a concentrated electrolyte,  $E_{\text{con}}$ , up to the breakdown was followed by another in a diluted electrolyte,  $E_{\text{dil}}$  (regions I and II, respectively). As can be observed in Figure 6b, in the region II the breakdown process is stopped and the voltage curve starts to increase at the last voltage attained in region I at a rate characteristic of the second electrolyte, until it reaches a higher breakdown voltage, typical of this last electrolyte ( $320$  V). A new change to the first electrolyte ( $E_{\text{con}}$ , Figure 6c) leads to the  $V(t)$  curve corresponding to the concen-

(4) Albella, J. M.; Montero, I.; Martínez-duart, J. M. *Electrochim. Acta* **1987**, *32*, 255.

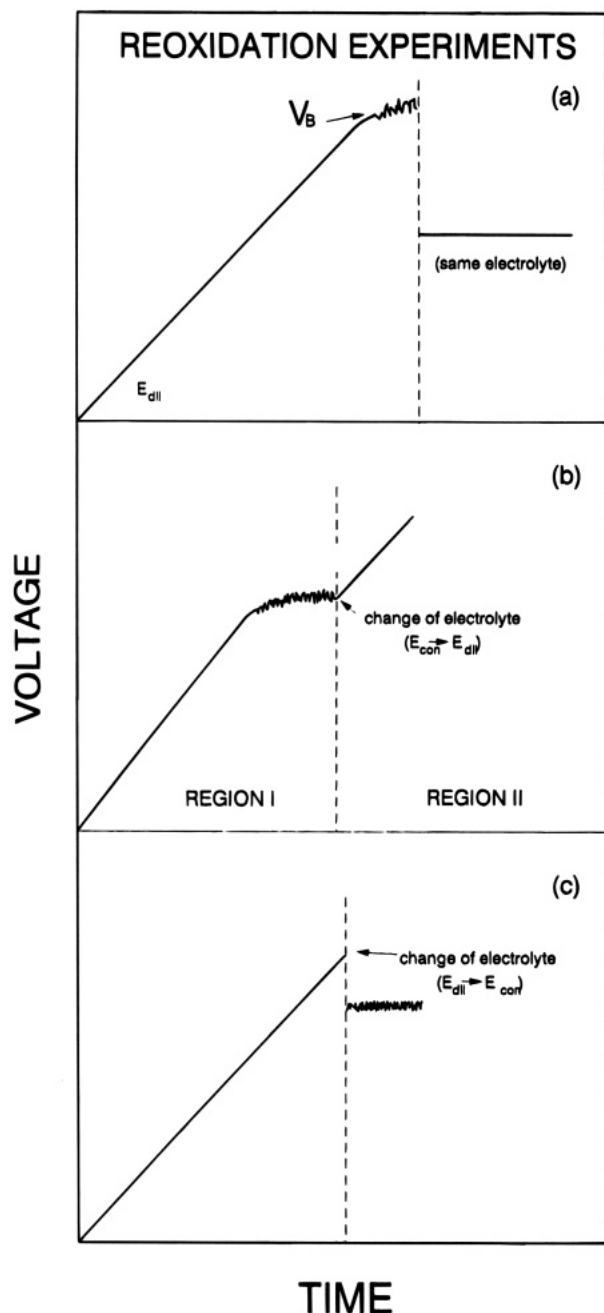


**Figure 6.** Voltage-time curves corresponding to “double-anodization” experiments: (a) anodization up to breakdown voltage followed by reanodization at a lower voltage in the same electrolyte. (b) Anodization in a concentrated electrolyte ( $E_{con}$ ) followed by reanodization in a dilute electrolyte ( $E_{dil}$ ). (c) Inverse process, anodizing first in the diluted and then in the concentrated electrolyte.

trated electrolyte and gives rise to a decrease of the anodization voltage toward the value corresponding to this electrolyte, with a sudden occurrence of breakdown.

The question at this point is to know what occurs in the oxide during the second stage of the oxidation. In a previous paper<sup>5</sup> we studied the breakdown damage caused in the first stage through quantification of the  $V(t)$  reoxidation curve. In this work the healing effect of the reoxidation process on the sample has been directly observed. As can be appreciated from the

(5) Montero, I.; Fernandez, M.; Albella, J. M. *Electrochim. Acta* **1987**, *32*, 171.

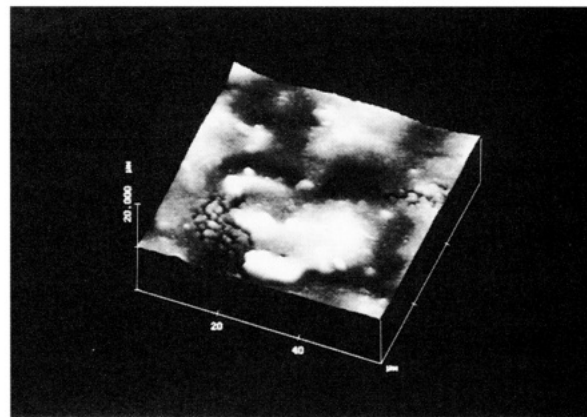


**Figure 7.** A  $60 \times 60 \mu\text{m}^2$  3D representation of AFM image of the sample reanodized at the conditions specified in Figure 6a.

comparison of the surface morphology in a “gray” sample (Figure 3) and in the same sample after reanodization under the conditions indicated in Figure 6a (Figure 7), the branched microfissures have partially disappeared in the latter, showing wide regions of flat areas. In addition, the initial roughness produced on anodic  $\text{Ta}_2\text{O}_5$  films subjected to breakdown is smoothed (Figure 4). Thus, the values of the rms roughness of  $25 \times 25 \mu\text{m}^2$  images measured before and after the reoxidation process are 327 and 297 nm, respectively. The decrease of the roughness is associated to the formation of oxide into the cracks and pores during the reoxidation process.

### Discussion

The above results can be explained in light of the breakdown models postulated for ideal systems (like  $\text{Ta}_2\text{O}_5$  and  $\text{Al}_2\text{O}_3$ ) during the anodic oxidation. These models are generally based on avalanche mechanisms established for insulating films flanked by metallic contacts. The electrons injected at the oxide/electrolyte interface are accelerated by the high electric field of anodization (in the range  $6 \times 10^6 \text{ V cm}^{-1}$ ) and then grow in avalanches as a consequence of the ionization of the lattice ions by the impacts of the electrons.<sup>6-8</sup> The avalanche electronic current developed at some definite spots of the sample surface gives rise to a local Joule heating, leading eventually to breakdown when the avalanche current reaches a critical size.

Shimizu et al. have suggested that, in a first stage, the local Joule heating increases the ionic current at these sites and may cause an “overgrowth” of the film, in the form of small dome-shaped protuberances on the oxide surface.<sup>7</sup> The granular structure and the protrusions observed in Figure 1 can be attributed to this effect. These authors further assume that the accumulated heat at these points increases the probability of propagation of the damage, thus inducing other effects such as evaporation or crystallization of the film. Structural changes in the morphology in the form of cracks and microfissures extended all over the surface, as depicted in Figure 2, are then expected after the initial stages of breakdown, not discarding the possibil-

(6) Albella, J. M.; Montero, I.; Martinez-duart, J. M. *Thin Solid Films* **1985**, *125*, 57.

(7) Shimizu, K.; Thompson, G. E.; Wood, G. C. *Thin Solid Films* **1982**, *92*, 231.

(8) Kadary, V.; Klein, N. *J. Electrochem. Soc.* **1980**, *127*, 139.

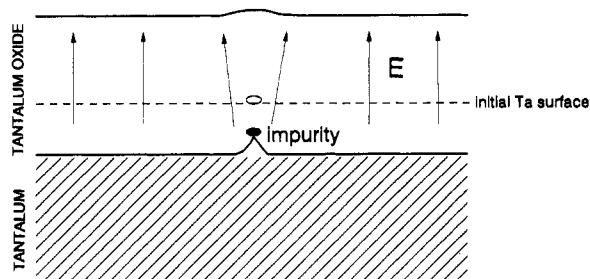


**Figure 8.** Sketch of the local electric field enhancement at the impurity sites left on the receding Ta surface during anodization.

ity of mechanical failure as a final step. In light of these ideas and taking into account the stochastic character of the avalanches (both in space and time) predicted by Kadary and Klein,<sup>8</sup> Figures 1 and 2 can be regarded as instantaneous pictures of the succession of the breakdown events at different times, including the presence of incipient small grains, grains of larger sizes and some other protuberances and ridges and finally the resulting cracks and microfissures.

The differences observed in Figures 1, 2, and 5 for the breakdown damage indicate that the breakdown processes are strongly dependent on the state of the initial tantalum surface. In samples only degreased (Figure 5), the localized breakdown spots aligned along the grooves can be associated to the impurities left behind on the surface by the rolling process, which also give low breakdown voltages. The reduction of the breakdown voltage in these samples can be related to the local electric field enhancement at the protuberances created on the receding Ta surface at the impurity sites (see sketch of Figure 8). On the other side, chemically polished samples, with a lesser defect concentration on the surface, grow to higher thicknesses before breakdown and present a lower concentration of pores and microfissures. However, the high density of grains observed on the flat areas of the surface, which have been associated to the onset of breakdown, gives an insight that this process is of an intrinsic nature, i.e., characteristic of the material.

Different authors have shown that the anodic films of tantalum present a double-layer structure, as a consequence of the electrolyte incorporation (phosphate ions) during the oxidation process.<sup>9,10</sup> The incorporated phosphorus species are homogeneously distributed through the outer oxide layer, whereas the inner layer can be considered pure Ta<sub>2</sub>O<sub>5</sub>. The thickness of the outer phosphorus-doped layer depends on the anodization conditions, but roughly it represents 60% of the whole thickness of the film. The presence of the electrolyte ions in the outer layer severely affects the physicochemical properties of the layer, in particular the recrystallization rate induced either by electric field or by thermal heating.<sup>11,12</sup> Thus, it is reasonable to assume that the outer layer of the film is more prone

to the structural changes produced by the discharges than the inner purer layer. As described above, the AFM pictures seem to demonstrate that the depth of the fissures nearly coincides with the thickness of this outer layer. This would prove the formation of non-shortening pores, according to the results obtained in another work.<sup>5</sup>

Following this model, in a previous work we envisaged the first stages of the breakdown phenomena as an alternative sequence of pore formation across the outer layer of the film and pore refilling with new oxide at the discharge spots.<sup>5</sup> Furthermore, the size of the electronic avalanches critically depends on the magnitude of the primary electron current injected at the electrolyte/oxide interface. Different authors have postulated that the value of the primary electron current is proportional to the inverse of the resistivity or the concentration of the contacting electrolyte following a power law.<sup>13,14</sup> Therefore, the change of electrolyte once the samples have been previously broken down immediately produces a new oxide layer with the formation of the concurrent avalanches pertaining to the new electrolyte.<sup>5,6</sup> This explains the "double anodization" experiments and the corresponding curves of Figure 6, i.e., healing of the breakdown spots when the oxide is reformed in the same electrolyte (Figure 6a), formation of new oxide layers if the reoxidation is performed in a more diluted electrolyte (Figure 6b) and breakdown at a lower voltage of a sample grown at higher voltage when the electrolyte is made more concentrated (Figure 6c). It is important to remark that although some of the breakdown spots can be healed during further anodization, continuous Joule heating at these spots probably increases the damage and gives the characteristic "gray oxide" observed in Figure 3.

## Conclusions

The first stages and the evolution of the breakdown phenomena during the anodic oxidation of tantalum have been studied by atomic force microscopy. This technique has proved to be a powerful tool to study the initial stages and the evolution of the breakdown damage during prolonged anodization. Of particular interest is the observation of a fine granular structure scattered across the surface, difficult to detect by other means. These sites can be considered as the first evidence of the onset of breakdown. According to the ideas of Shimizu et al. the incipient breakdown spots are explained as an overgrowth of the film due to the Joule heating produced by the local avalanches.<sup>7</sup> These small features subsequently grow in size and develop into cracks and microfissures likely as a consequence of mechanical failure. In the first stages, the breakdown damage may be healed by the formation of new oxide layers at the discharge spots, but after prolonged anodization the damage is extended in wide areas with the production of a microcrystalline powder characteristic of "gray oxide". It is found that the morphology of the bare tantalum foil can determine the characteristics of the breakdown damage. As-received samples present lower breakdown voltages with the formation of local-

(9) Randall, J. J.; Bernard, W. J.; Wilkinson, R. R. *Electrochim. Acta* **1965**, *10*, 183.

(10) Montero, I.; Albella, J. M.; Martinez-Duart, J. M.; Soriano, L. *J. Mater. Sci.* **1987**, *22*, 1785.

(11) Pawel, R. E.; Campbell, J. J. *J. Electrochem. Soc.* **1980**, *127*, 2035.

(12) Dell'Oca, C. J.; Pulfrey, D. L.; Young, L. In *Physics of Thin Films*; Academic Press: New York, 1971; Vol. 6.

(13) Ikonopisov, S. *Electrochim. Acta* **1977**, *22*, 1077.

(14) DiQuarto, F.; Piazza, S.; Sunseri, C. *J. Electroanal. Chem.* **1988**, *248*, 99.

ized pores, likely associated with the impurities left behind by the rolling process, whereas chemically etched samples offer higher breakdown voltages and the attack appears in the form of grains and microfissures which, under long polarization times, are extended across the surface.

The results also reveal that the breakdown damage seems to affect only the outer oxide layer, producing pores or fissures nonshorting the underlying metal. In accordance with previous data,<sup>5</sup> this effect is provoked by the presence of the electrolyte species (phosphate anions) incorporated into the outer layer of the film.

Furthermore, the healing effects on the damaged areas has been followed by "double anodization" experiments, by reanodizing the samples under different conditions. The AFM images of samples reanodized at a lower voltage show in this case that the damage partially disappears giving a much lower rms surface roughness.

**Acknowledgment.** This work has been supported by the "Comisión Interministerial de Ciencia y Tecnología" (CICYT) of Spain, project no. MAT 92-0093.

CM9501590